The 1992 Tafilalt seismic crisis (Anti-Atlas, Morocco)

Ihsane Bensaid, Taj-Eddine Cherkaoui, Fida Medina, Bento Caldeira, Elisa Buforn, Anas Emran & Youssef Hahou

Journal of Seismology

ISSN 1383-4649
Volume 16
Number 1

J Seismol (2012) 16:35-53
DOI 10.1007/s10950-011-9248-5

Springer

J Seismol (2012) 16:35–53
DOI 10.1007/s10950-011-9248-5

ORIGINAL ARTICLE

The 1992 Tafilalt seismic crisis (Anti-Atlas, Morocco)

Ihsane Bensaid · Taj-Eddine Cherkaoui · Fida Medina · Bento Caldeira · Elisa Buforn · Anas Emran · Youssef Hahou

Received: 1 November 2010 / Accepted: 25 August 2011 / Published online: 10 September 2011

Abstract The Tafilalt region, located at the eastern end of the Anti-Atlas chain in Morocco, was shaken on 23 and 30 October 1992 by two moderate earthquakes of magnitude *mb*~5 and intensity~VI MSK64, which caused two deaths and great damage in the area between Erfoud and Rissani. The review of data available on the seismic crisis allowed us to improve the knowledge on the macroseismic, instrumental and source parameters of the earthquakes. The main results of the present study are: (1) location of the epicentres with the help of data from a close portable network allowed us to propose new epicentral coordinates at 31.361° N, 4.182° W (23 October) and 31.286° N, 4.347° W (30 October); both events have focal depths of 2 km; (2) the shock of 30 October was followed by a series of 305 aftershocks, most of which were located west of Rissani; the 61 best-constrained events had focal depths of 5 to 19 km and magnitudes 0.7 to 3; (3) the largest damage was located in an area between the two epicentres within the Tafilalt valley and was probably amplified by site effects due to the proximity of the water table within the Quaternary sediments; (4) focal mechanisms of the main events correspond to strike-

I. Bensaid
Département des Sciences de la Terre, Institut Scientifique, Laboratoire de Physique du Globe, Equipe Sismologie et Magnétisme, Université Mohammed V-Agdal, Rabat, Morocco

I. Bensaid
Ecole Mohammedia d'Ingénieurs, Université Mohammed V-Agdal, Rabat, Morocco

T.-E. Cherkaoui
Département des Sciences de la Terre, Institut Scientifique, Rabat, Morocco

F. Medina (✉) · A. Emran
Département des Sciences de la Terre, Institut Scientifique, Laboratoire de Géologie et Télédetection (associé CNRST URAC 46), Equipe Télédétection, Ressources et Risques naturels, Université Mohammed V-Agdal, Rabat, Morocco
e-mail: medina@israbat.ac.ma

B. Caldeira
Centro Geofísico, Universidade de Evora, Evora, Portugal

E. Buforn
Departamento de Geofisica y Meteorologia, Universidad Complutense, Madrid, Spain

Y. Hahou
Centre National pour la Recherche Scientifique et Technique, Institut National de Géophysique, Rabat, Morocco

slip faulting with fault planes oriented N–S (left lateral) and E–W (right lateral); the only mechanism available for the aftershocks also corresponds to strike-slip faulting; (5) spectral analysis shows that the scalar seismic moment (*Mo*) of the first event is slightly larger than the second; the corresponding values of *Mw* are 5.1 and 5.0, respectively; (6) the dimensions of the faults for a circular fault model are 7.7±1.4 and 7.4±1.2 km, respectively; the average displacement is 4 cm for the first event and 3.7 cm for the second; the stress drop is 0.4 and 0.3 MPa, respectively, in agreement with standard values; (7) the Coulomb Stress test performed for both earthquakes suggests a relationship between both events only when the used location is at the limit of the horizontal uncertainty; (8) finally, the occurrence of these shocks suggests that the Anti-Atlas is undergoing tectonic deformation in addition to thermal uplift as suggested by recent publications.

Keywords Maghreb · Seismology · Seismotectonics · Focal mechanisms · Rissani · Fault dimension · Coulomb stress

1 Introduction

In the Ibero-Maghrebian area, the present-day convergent plate motion of the Nubian plate with respect to Iberia occurs along a NW–SE trend, as inferred from plate kinematics (DeMets et al. 2010), focal mechanism solutions (Medina 1995; Buforn et al. 1995, 2004; Henares et al. 2003; Medina and El Alami 2006; Stich et al. 2006; de Vicente et al. 2008; Pedrera et al. 2011) and GPS observations (McClusky et al. 2003; Vernant et al. 2010). An almost perpendicular NE–SW motion occurs in the central Rif and its foreland (Fadil et al. 2006; Stich et al. 2006; Tahayt et al. 2009; Vernant et al. 2010) in relation to a SW-verging tectonic escape process (Chalouan et al. 2006). The total NW–SE convergence rate of 4 mm year^{-1} includes the rates observed especially at recent chains such as the Rif, and the High Atlas (~1 mm year^{-1}). The shortening is in great part accommodated by earthquakes of low to moderate magnitude (maximum *Mw*=6.3 at Al Hoceima in 2004) and generally shallow foci (Ben Sari 1978; Hatzfeld 1978; Frogneux 1980; Cherkaoui 1988, 1991; Bezzeghoud and Buforn 1999; El Alami et al. 2004), although a few events have focal depths of 100 km beneath the Middle Atlas (Hatzfeld and Frogneux 1981; Cherkaoui 1991) and in northwestern Morocco and adjacent Alboran area (Cherkaoui 1991; Buforn et al. 2004).

South of the High Atlas active belt, the Anti-Atlas (Fig. 1) has been classically considered as a relatively stable area from the neotectonic and seismic aspects because of the absence of major deformations and historical records of major earthquakes (Roux 1934; Elmrabet 2005), although some small shocks were recorded during the last century (Cherkaoui 1988).

Despite the alleged stable character of the Anti-Atlas, the Tafilalt region, located at its eastern termination, was shaken on 23 and 30 October 1992, by two moderate earthquakes of magnitude *mb*~5 and intensity VII MSK64 (Cherkaoui 1993), which caused two deaths and great damage in the area between Erfoud and Rissani (Fig. 2a). Several questions were arisen by these events as to: (1) the occurrence of earthquakes and the nature of present-day tectonics in this stable area; (2) the remarkable lack of aftershocks after the 23 October earthquake and the long series after the 30 October shock and (3) the possible spatial relationship of both events.

Focal mechanisms for both shocks were determined by Harvard Centroid Moment Tensor (CMT solutions) and by Jabour (1993) for the shock of 23 October (waveform analysis), suggesting strike-slip faulting along N–S left-lateral and E–W right-lateral planes. However, as Harvard CMT and Jabour's solutions appeared to be inconsistent with available P wave data at regional distances, due to the use of teleseismic data and a fixed depth (15 km) for shallow earthquakes, we searched new solutions based on P wave first motion data. Another important point was the difference on focal parameters, especially on focal depth, that varies from 5 to 29 km. The preliminary results of our investigations (Bensaid et al. 2009) led us to review all the data available on both events and their effects, using new and older unpublished seismological surveys and reports, geological updates provided by hydrocarbon exploration research on the structure of the region and geophysical studies across the Atlas chain.

In the following sections, we review the focal parameters (hypocentral relocation, energy), macroseismic effects, aftershock distribution and the source parameters such as fault-plane solution, scalar seismic

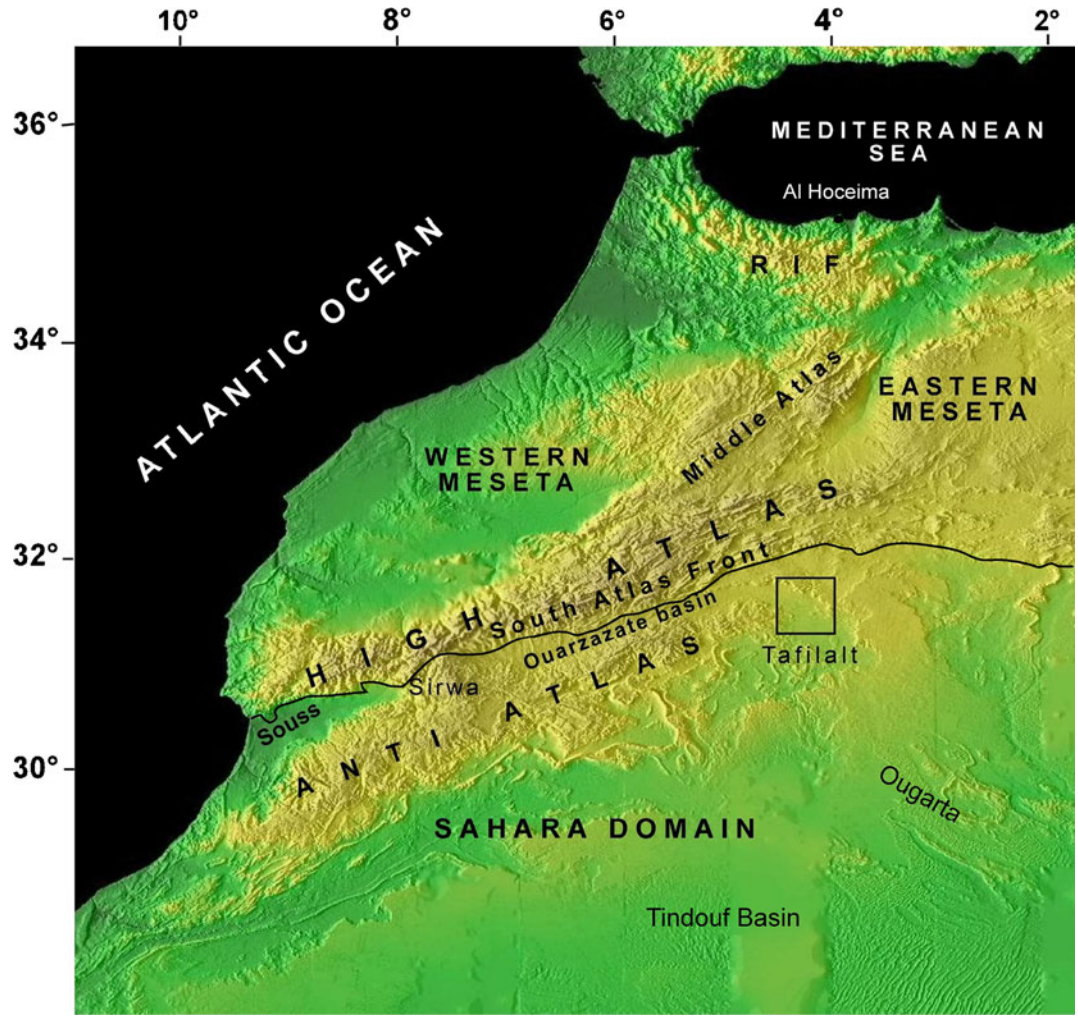

Fig. 1 Structural domains of Morocco (topography from NOAA) and location of the Tafilalt valley (*inset*)

moment, source dimension, the average displacement and the stress drop. Then, we discuss the validity of the data and the possible relationship between both earthquakes and the implications on the tectonics of the Anti-Atlas chain.

2 Geological setting

The Anti-Atlas chain extends ENE-WSW for about 700 km, from the Atlantic coast in the west to the Tafilalt region in the east (Fig. 1). To the north, the Anti-Atlas is separated from the seismically active High Atlas intra-continental chain by the South Atlas Front and the Ouarzazate and Souss foreland basins, except at the Sirwa promontory, a thermally driven plateau (e.g. Missenard et al. 2006). To the south, the chain is bounded by the Tindouf basin, which is considered as a post-Turonian lithosphere syncline by Frizon de Lamotte et al. (2009). Eastwards, the Anti-Atlas is relayed by the NW–SE trending Ougarta chain.

The Anti-Atlas formations consist of a Precambrian crystalline and sedimentary basement overlain by a thick (~4–9 km) Palaeozoic sedimentary cover and thin Mesozoic and Cenozoic sediments (e.g. Choubert et al. 1946–1955; Gasquet et al. 2008; Michard et al. 2008). The uplift of the Anti-Atlas is related to the former High Atlas rift, when it formed its southern shoulder during the Triassic–Jurassic (Frizon de Lamotte et al. 2009) and more recently to the High Atlas orogeny since the Middle Eocene (Malusà et al.

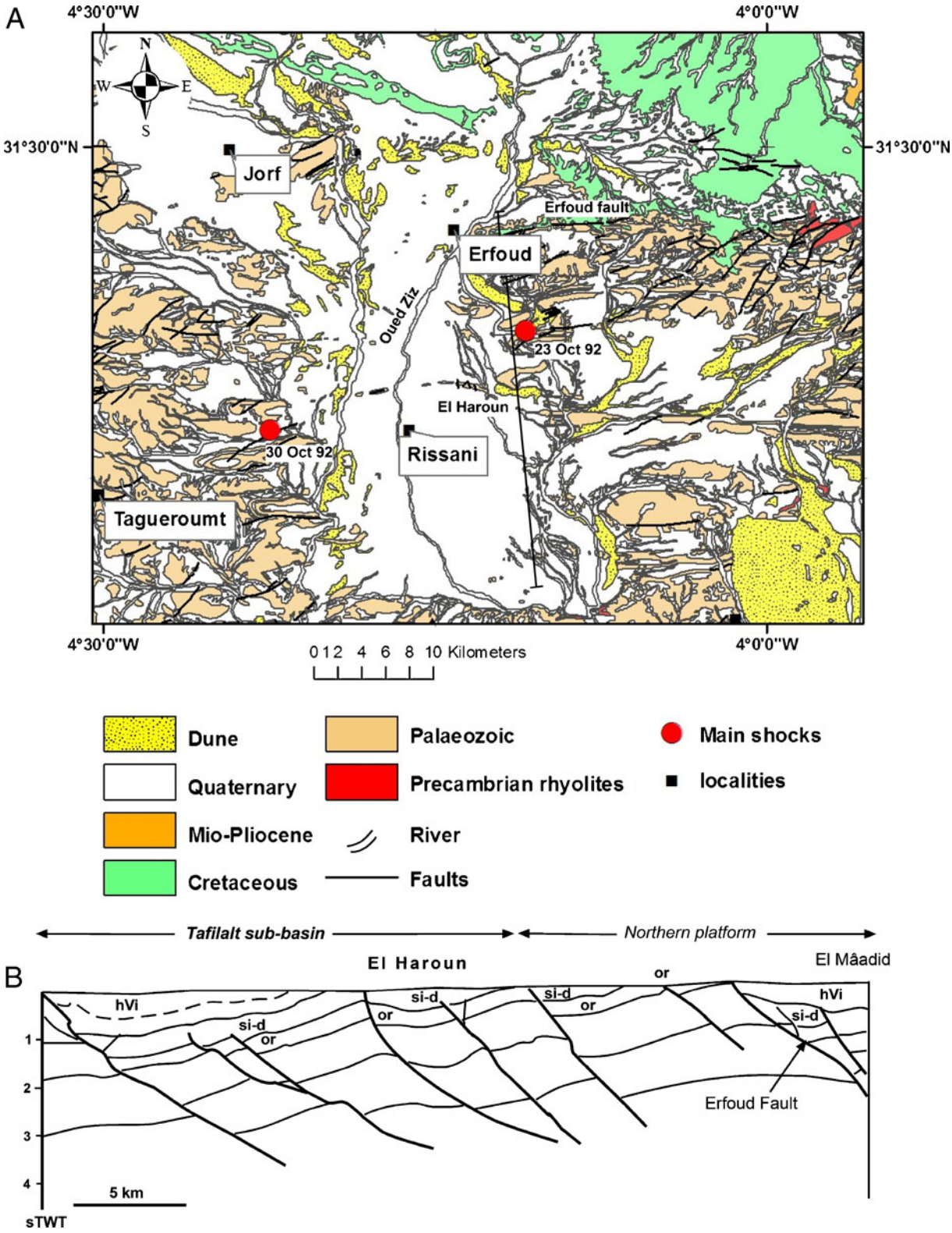

◀ **Fig. 2** **a** Geological map of the Tafilalt valley (location in Fig. 1). Geological contours and faults were taken from the maps of Margat (1960) and Destombes and Hollard (1986), georeferenced and vectorized by GIS tools and superimposed to Landsat image p200r38_5t871007 (7/10/1987) obtained from Global Land Cover Maryland University (http://glcf.umd.edu/data/landsat/); **b** simplified N–S seismic section (RS08) across the Tafilalt valley (after Robert-Charrue and Burkhard 2008, simplified and completed; location in (**a**)) *or* Ordovician; *si-d* Silurian and Devonian; *hVi* Lower Carboniferous

2007) and to an asthenospheric dome since the Miocene (Teixell et al. 2005)

Regionally, the area between Erfoud and Rissani is located along the oued Ziz and oued Rheriss common valley, which runs N–S, perpendicular to the E–W trend of the Eastern Anti-Atlas segment. The geological formations in the area (Fig. 2a) consist of Precambrian rhyolites and andesites, overlain by a folded and faulted cover of Cambrian through Carboniferous sedimentary formations, and unconformable Cretaceous flat-lying deposits affected by a few faults (Margat 1960; Destombes and Hollard 1986).

The recent formations in the valley belong to several cones, with up to 30 m thick Quaternary alluvial and lacustrine deposits. Above the Palaeozoic basement, the lowermost deposits consist of marls, lacustrine carbonates, gravels and conglomerates of Tensiftian age (late Middle Pleistocene; 150–300 ky according to the scale of Plaziat et al. 2008), overlain by clays, gravels and silts (Margat et al. 1962) of Soltanian age (latest Pleistocene; 10.5–32 ky). The uppermost levels, on which the villages are generally built, consist of 10 m thick clays.

The main tectonic events can be summarized as follows (Toto et al. 2007; Malusà et al. 2007; Baidder et al. 2008; Frizon de Lamotte et al. 2009): (1) a syndepositional extensional regime from Cambrian to Early Carboniferous times, which produced E–W striking, northward- or southward-dipping normal faults; (2) a Late Carboniferous through Permian NE–SW compression leading to E–W trending folds and reverse faults; (3) an erosional period until the deposition of Cenomanian-Turonian carbonates of the Hamada and Kem-Kem; (4) rapid uplift during the Neogene.

The shallow structural pattern (≤5 km) is clearly visible from field mapping (Baidder et al. 2008) and published ONAREP seismic-reflection profiles RS-8 (Baidder 2007; Robert-Charrue and Burkhard 2008), RS-6 and RS-10 (Toto et al. 2007). Despite contradictory interpretations, one of the common structures is the E–W striking Erfoud fault, which can be considered as a major detachment fault that bounds to the north the structural high located east and southeast of Erfoud (Fig. 2b). This fault separates the southern structural high from the Carboniferous basin located to the north. According to Baidder (2007) and Robert-Charrue and Burkhard (2008), the internal structure of the high consists of a Precambrian through Devonian series, affected by northward- or southward-dipping normal faults separated by tilted half-grabens. The strata close to the faults are folded, probably as forced folds related to the motion on faults, but some details point to later reactivation of the structures by Variscan, and probably later alpine compressional tectonics. The interpretation of Toto et al. (2007) emphasizes compressional tectonics, but normal faults were also interpreted south of the Erfoud fault.

At depth, the seismic refraction (Wigger et al. 1992) and electrical resistivity (Schwarz et al. 1992) measurements show that the Moho discontinuity is at 20 km depth and that the crust is of low P wave velocity (6.0 km s^{-1}) between 12 and 20 km depth at Erfoud. This conspicuous structure is interpreted as a major, northward dipping detachment, which extends far beneath the High and Middle Atlas chains (Giese and Jacoshagen 1992).

Neotectonics in the area is relatively mild (Joly 1962); the main structures are the large ENE–WSW-folds affecting the whole Anti-Atlas, and those located along the South Atlas Front (SAF) which may be locally important, with thrusting of Cretaceous deposits onto Quaternary terraces (Malusà et al. 2007). South of the SAF, the Cretaceous strata appear to be just slightly affected by the deformations related to the High Atlas orogeny (Zouhri et al. 2008). Close to Erfoud, Rousseau et al. (2006) reported the presence of a 300-ka travertine (the Irdi travertine), which displays dislocations which may be related to palaeoseismicity (Plaziat et al. 2008). These deformations may also be related to remote seismic activity, as that of the SAF. Recent fission track and tectonic studies by Malusà et al. (2007) in the Saghro and Ougnat areas 90 km west of the Tafilalt valley show that after a slow Mesozoic uplift, the Anti-Atlas underwent fast exhumation (~2 km) since the Miocene. The NNE–SSW to NNW–SSE compressional structures observed in the field along ENE–WSW trending faults are assigned to the Late Neogene to Present-day tectonics.

3 Seismicity

3.1 Regional seismicity

Seismicity of Morocco is characterized by the occurrence of low to moderate earthquakes at shallow depth (less than 40 km). Distribution of earthquakes with magnitudes ≥3.0 in Morocco and surrounding areas for the period 1970–2010 are shown in Fig. 3a. Data were taken from the file of Moroccan events for the 1901–1984 period (Cherkaoui 1988), completed by shocks recorded from 1985 to 2010. Most epicentres are located at the northern part of Morocco and are associated to the E–W plate boundary between Eurasia and Nubia and roughly following the Mediterranean coast (see the recent review by Buforn and Udias 2010). The most seismic region is the Al Hoceima area, where two damaging earthquakes occurred in 1994 (Mw=6.0) and 2004 (Mw=6.3). A second alignment of epicentres corresponds to shocks located in the High Atlas. Most earthquakes have shallow depths (less than 40 km) and only some, located in the Atlas and Northwest Morocco, have foci at intermediate depth (70 km<h<153 km) (Hatzfeld and Frogneux 1981; Cherkaoui 1991; Buforn et al. 2004). This intermediate depth seismicity is not related to any subduction zone in the Atlas, as indicated by surface geology (Seber et al. 1996).

The 23 and 30 October earthquakes (Fig. 3a, b) are located south of High Atlas in the Tafilalt region, characterized by a low seismic activity, as inferred from the Moroccan catalogue 1901–1984 (Cherkaoui 1988), completed for the period 1985–2010. In this region, most epicentres are associated to the High Atlas and correspond to moderate (magnitude less than 5.0) shallow events (h<40 km). However, some earthquakes occur south of the Atlas Front (the Boumalne–Tineghir–Goulmima line; Fig. 3b), the largest are the 23 and 30 October 1992 earthquakes. In this region, from 1901, 15 earthquakes have reached maximum intensities V MSK, but only four have caused severe damage: the Assoul 1960 (mb=4.7 and Io=VI) and 1986 (mb=4.9 and Io=V) earthquakes, and the 1992 Rissani shocks. In terms of magnitude, the larger earthquake that occurred in the area previously to the 1992 shocks is the 1994 event (mb=4.6) located south of Boudenib.

An important problem for the seismic survey of this region is the instrumental errors on the hypocentral determinations, due to the large distance to the Moroccan permanent seismological networks; the nearest station, installed in 1973, is located in Hassan Addakhil dam, at 27 km NW of Errachidia, and about 80 km north of Rissani (H.A. in Fig. 3b). However, this station underwent severe technical problems, which led to frequent periods of interruption of recording.

Fig. 3 **a** Seismicity of Morocco and surrounding areas from 1970 to 2010 (magnitude M≥3.0). Data for the period 1970–1984 are based on Cherkaoui (1988) catalogue, completed with events recorded between 1985 and 2010. *1*, *2* the 23 and 30 October Rissani earthquakes, respectively. **b** Seismicity of southwestern Morocco for the period 1901–2010. *H.A. Dam* Hassan Addakhil dam

3.2 The 23 and 30 October 1992 earthquakes

There are different hypocentral determinations for the 23 and 30 October earthquakes. In Table 1, hypocenters estimated by the International Seismological Centre (ISC; ISC 1992), NEIC and Hahou et al. (2003) are given. In this study, we have carried out a new location for the 23 and 30 October shocks based on additional data collected from 16 short-period vertical-component portable stations installed by the Institut Scientifique team near Khénifra (200 km NW of Erfoud) from 29 September to 30 October 1992.

The hypocentral locations were determined using the revised version of the HYPO71 computer programme (Lee and Valdés 1985) and a standard velocity model for Morocco with V_p/V_s=1.74 (Frogneux 1980). The epicentral coordinates are 31.361° N, 4.182° W (23 October) and 31.286° N, 4.347° W (30 October) (Fig. 3b). These new locations (Table 1) show similar ERH values (4.0 and 5.0 km) to those of ISC (4.2 km in both cases), but lower ERZ (5.2 and 6.0 km versus 9.6 km). The RMS (0.54 and 0.7 s) are also lower in comparison to those of NEIC (1.08 and 1.23 s) and ISC (1.13 and 1.33 s).

A remarkable fact is that the network installed by the CNRST from 24 to 28 October in the epicentral area after the first shock and composed by five analogue short period stations (Kinemetrics Instrument Model PS-2) located in an area of 100 km^2 in the epicentral area did not record any aftershock (Hahou 2005).

The Khénifra portable network was transferred to the Rissani area immediately after the 30 October

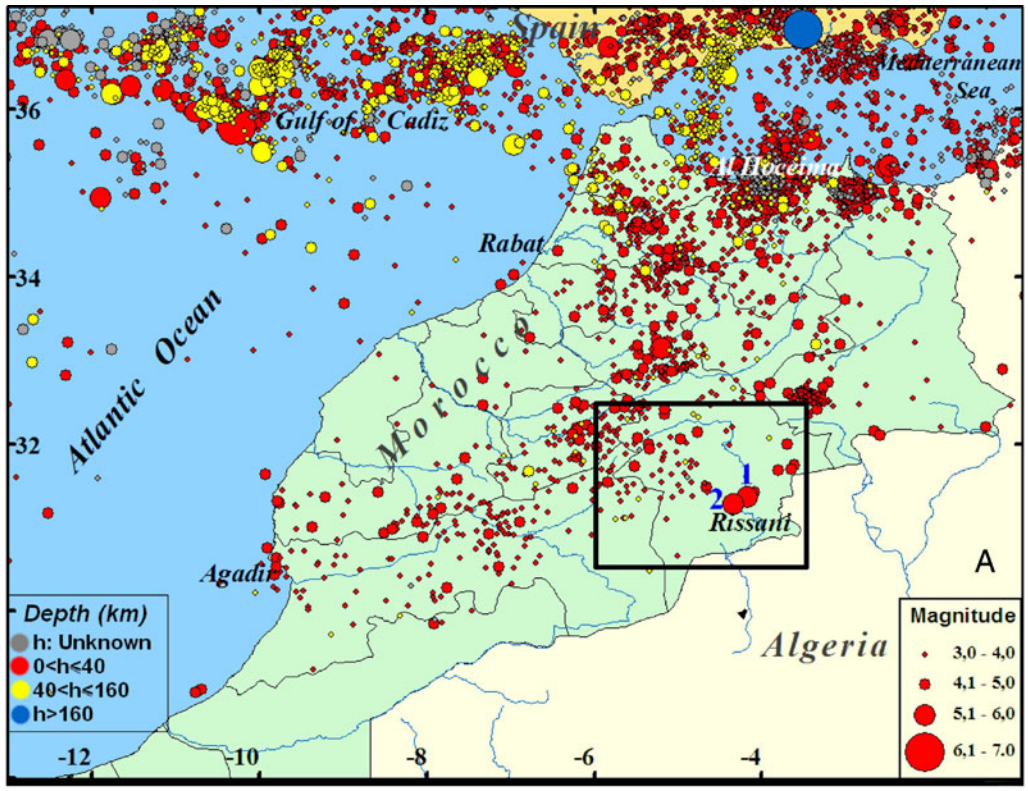

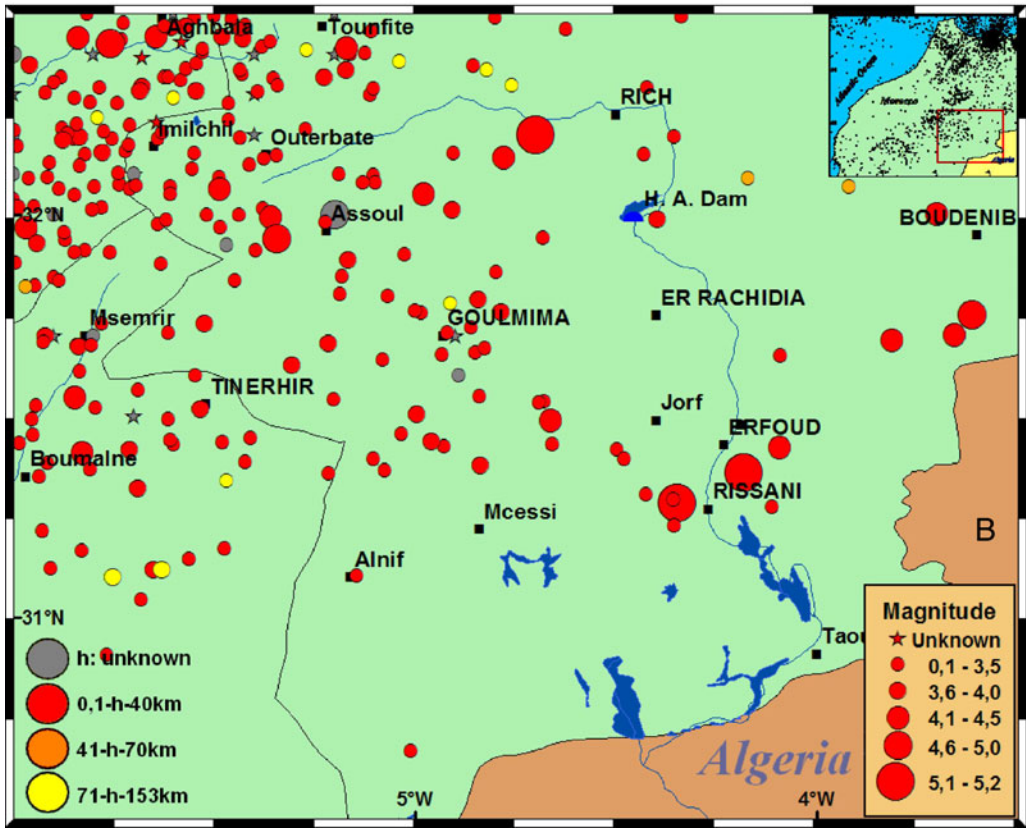

Table 1 Location of the main shocks by different institutions and authors

Date	Origin time	Coordinates		Depth (km)	Magnitude	RMS (sec)	Author
		Lat N Long W	ERH				
23 Oct 1992	09:11:09.0	31.355°–4.318°		28.6	*mb*=5.3 Mw=5.6	1.08	NEIC
	09:11:05.5	31.294°–4.325°	4.2	5.4±9.6	*mb*=5.2	1.13	ISC
	09:11:12.0	31.466°–4.116°		14	*Md*=5.2		Hahou et al. 2003
	09:11:08.5	31.361°–4.182°	4.0	2.0±5.2	*Md*=5.2	0.54	This paper
30 Oct 1992	10:43:58.4	31.284°–4.372°		25.6	*mb*=5.1 Mw=5.6	1.23	NEIC
	10:43:55.8	31.246°–4.381°	4.2	8.0±9.6	*mb*=5.1	1.33	ISC
	10:44:02.0	31.432°–4.507°		16	*Md*=5.3		Hahou et al. 2003
	10:43:58.1	31.286°–4.347°	5.0	2.0±6.0	*Md*=5.1	0.7	This paper

ERH is the standard horizontal error in kilometres

shock. Nine portable analogical stations were installed in the main epicentral area. This network was operational from 31 October at 03:00 A.M. (UT) through November 8 (Fig. 4a). The Sprengnether MEQ 800 smoked-paper portable stations were connected to a 1-Hz vertical component seismometer and equipped with internal quartz clocks and a HBG antenna. The geometry of the network was chosen so as to cover the epicentral area (about 500 km^2) with an approximate meshing of 17 km. A preliminary report was carried out by Cherkaoui (1993).

A total of 305 aftershocks were recorded during the survey. The seismic activity was intense during the first 5 days, as reflected by the 85 events that were recorded on 1st November alone, but decreased afterwards, until becoming insignificant on 8 November with only one recorded event (Fig. 4b). Nine aftershocks were felt with intensities V to II MSK. The hypocentral locations were determined using the revised version of the HYPO71 computer programme (Lee and Valdés 1985) and a standard velocity model for Morocco with V_p/V_s=1.74 (Frogneux 1980). Magnitudes were calculated from signal duration using the formula:

$$Md = a + b\log(\tau) + c\Delta \quad (1)$$

Where τ is the signal duration (in seconds), Δ is the epicentral distance (in kilometres), and a, b, c are constants which were calculated for each station by the least squares method, using data recorded by the seismic permanent network of Morocco. For the latter, the magnitudes *Md* were calibrated against magnitudes *mb* determined by ISC and USGS (Cherkaoui 1988, 1991).

We selected 61 aftershocks whose hypocenters showed the least errors (RMS≤0.2 s; ERH and ERZ ≤2 km). Their magnitudes are from 0.7 to 3.0, and the focal depths are from 5.0 to 19.0 km (Fig. 4a), which probably is the limit between the upper crust and the lower crust. The aftershock distribution map (Fig. 4a) shows that the seismic activity was exclusively concentrated west of Rissani within an area of approximately 182 km^2 (13×14 km) with a distribution of epicentres in NW–SE direction.

A vertical E–W section across the aftershock area (Fig. 4c) shows an increase of the depth of foci towards the west; however, no precise relationship with faults could be delineated, because all the shocks are beneath the faults depicted in the seismic section of Fig. 2b, which is a time section.

4 Macroseismic data

The 23 October shock was felt within a large area south of the High Atlas and caused widespread damage. According to Hahou et al. (2003) the walls of most adobe constructions suffered large cracks or even partial destruction, while total collapse was observed in several cases. Other reported effects included rock falls in the High Atlas, ground fissures and cracks in the epicentral area and surrounding region. According to these observations, Hahou et al. (2003) assigned maximum intensity VIII (MSK) to the epicentral region.

The 30 October shock also was felt at a large distance (about 250 km from the epicentre). The

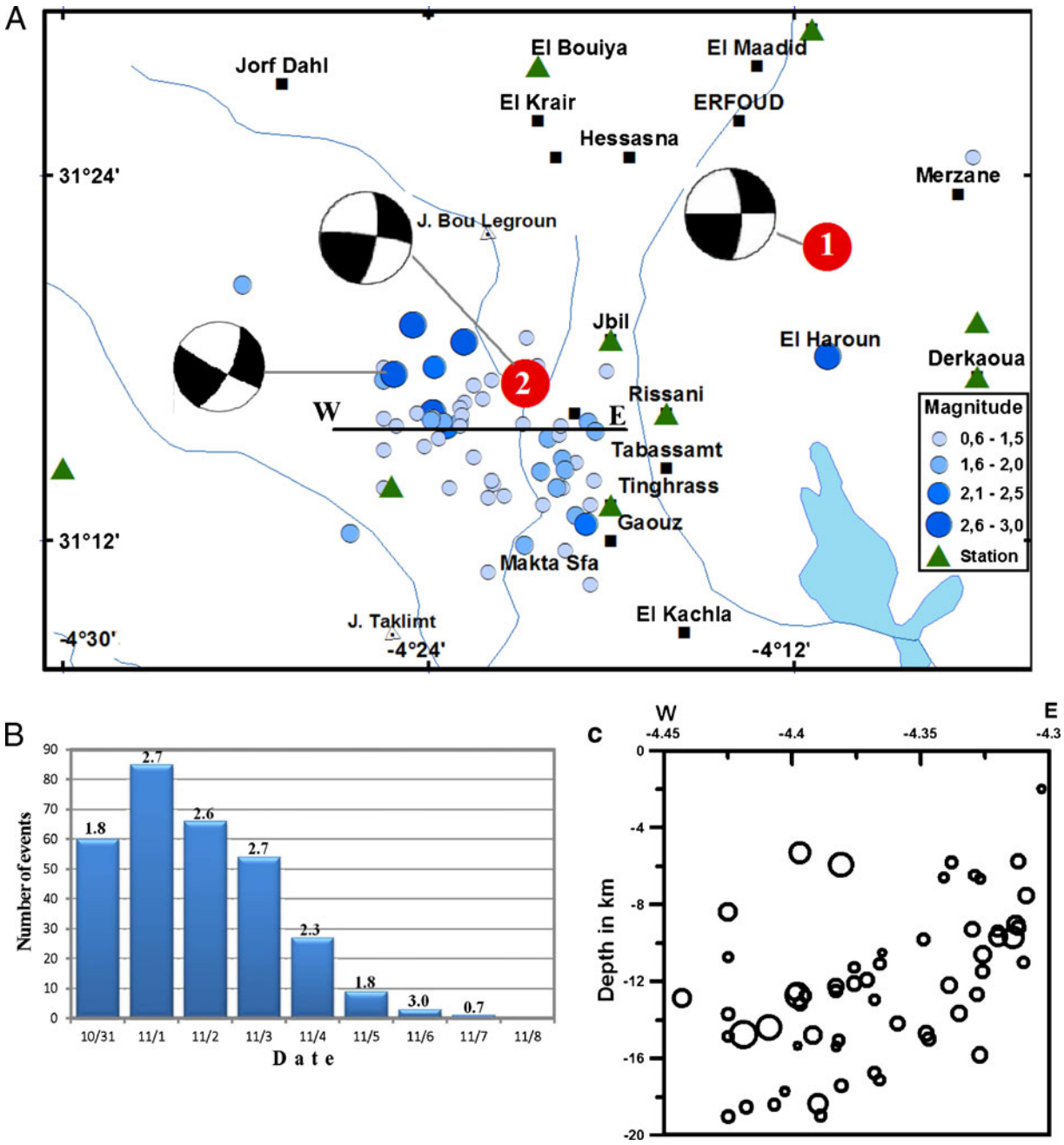

Fig. 4 **a** Distribution of 61 aftershocks recorded from 31 October to 8 November 1992 with the focal mechanisms for the main shocks (1 and 2) and the largest aftershock (*Md*=3.0) determined in this study. The *triangles* represent the temporary seismic stations installed in Rissani area. E–W the location of the vertical cross-section in (**c**). **b** Daily frequency of aftershocks (*Md*≥0.6) recorded from 31 October to 8 November 1992 by Cherkaoui (1993). The *numbers above the bars* correspond to the recorded maximal magnitudes per day. **c** Vertical E–W cross-section of the aftershock distribution (location in Fig. (**a**))

macroseismic study is based on 117 questionnaires together with a field survey and in situ observations of the damage produced within a radius of 30 km around the epicentre, with the exception of the western part because of the low population density. A problem in this study has been the correct separation of effects produced by the 23 and 30 October shocks. In consequence, some intensity

values assigned to the 30 October earthquake may be overestimated.

In order to evaluate the damages, the constructions were subdivided into three categories, based on their resistance to seismic shocks: (1) traditional buildings made of poor local materials (wood, adobe, cut stone and adobe); (2) more recent classical masonry buildings (massive stone); (3) modern reinforced concrete constructions. Constructions of category (1) represent more than 90% of the fortified villages (*Ksour*), and less in the cities of Erfoud and Rissani. Most constructions of this category were destructed or became uninhabitable, because of partial structural failure of roof and floors. Buildings in classical masonry (Category 2), e.g. individual houses, public buildings such as the hospital, schools and modern apartments with a correct seismic resistant structure, are predominant in Erfoud and Rissani. However, in Rissani, some recent public buildings (such as the police station, the tax office, the Hassan II secondary school and the youth club) were affected by large and extensive wall cracks, leading to their closure. Constructions of Category 3 did not suffer any damage.

The largest damage (I=VII and VI MSK64) was observed within an area of 2,000 km², oriented NW–SE, including the *ksour* of Hessasna, El Khandek, Hannabou, El Kraïr and El Bouiya (Fig. 5). This zone is located in between the epicentres of the 23 and 30 October shocks and may explain the large damage observed, because of its proximity to both epicentres. This could also reflect a site effect or a fault trend, as we will discuss later.

5 Focal mechanisms

Focal mechanisms of these events, were estimated by Harvard CMT solutions and by Jabour (1993) from P and SH waveform analysis (broadband station ANTO); they correspond to strike-slip faulting along N–S left-lateral and E–W right-lateral planes (Table 2). As the Harvard CMT and Jabour's solutions appeared to be inconsistent with P data at regional distances, we tried to construct a new fault-plane solution that takes into account the regional stations.

The used data correspond to the Khenifra temporary network installed in this area from 29 September to 30 October 1992 at 12 h UT, the permanent Institut Scientifique and CNRST networks and the Instituto Geografico Nacional (IGN, Madrid, Spain) stations at less than 1,000 km, together with Tunisian and Ivory Coast stations and some Geofon and Geoscope stations at epicentral distances between 1,000 and 2,500 km. Quality of first motions, as illustrated by Bensaid et al. (2009), varies from excellent (Moroccan network) to poor (some Tunisian stations). The stations were chosen so as to cover all quadrants of the focal sphere, especially the southern and south-eastern quadrants, which are generally poorly covered in most solutions for Moroccan earthquakes.

Fault plane solutions have been obtained from first motion of P waves, using the algorithm developed by Brillinger et al. (1980) to estimate fault plane orientation, their errors and score for both shocks. A crustal-specific model for Morocco, formed by two flat layers (12 and 18 km, respectively) with constant velocity 6.0 and 6.75 km s^{-1}, has been used to estimate the take-off angles for stations at regional distances (less than 1,000 km). These velocities are constrained by seismic refraction data from Schwarz and Wigger (1988) and Wigger et al. (1992). For stations at larger distances, we have used the IASPEI model.

The best solution for the 23 October shock (Table 2, Fig. 6) is based on polarity data corresponding to the permanent Institut Scientifique, CNRST, IGN and Geoscope networks, together with the Tunisian and Ivory Coast stations. It corresponds to strike-slip faulting with a small component of normal faulting. The fault planes are near the vertical (dip 71º and 89º, respectively) and oriented in N–S and E–W directions (strike 359° and 89°, respectively). The P and T axes are horizontal and oriented NW–SE and NE–SW, respectively. The solution is well constrained with estimations of P and T errors less than 15º, the total number of data is 30 and the score 0.97. With respect to Harvard CMT and Jabour's solution, ours shows an opposite direction of dip for the N–S plane, constrained by the position of stations TAM, LIC, ANTZ, CIA and EPRU.

The fault-plane solution for the 30 October shock (Table 2; Fig. 6) is based on 17 polarities corresponding to data of the Institut Scientifique, CNRST, IGN and Geoscope permanent networks together with temporary stations installed near Khénifra. It also shows strike-slip faulting with a small component of reverse motion. The fault planes are

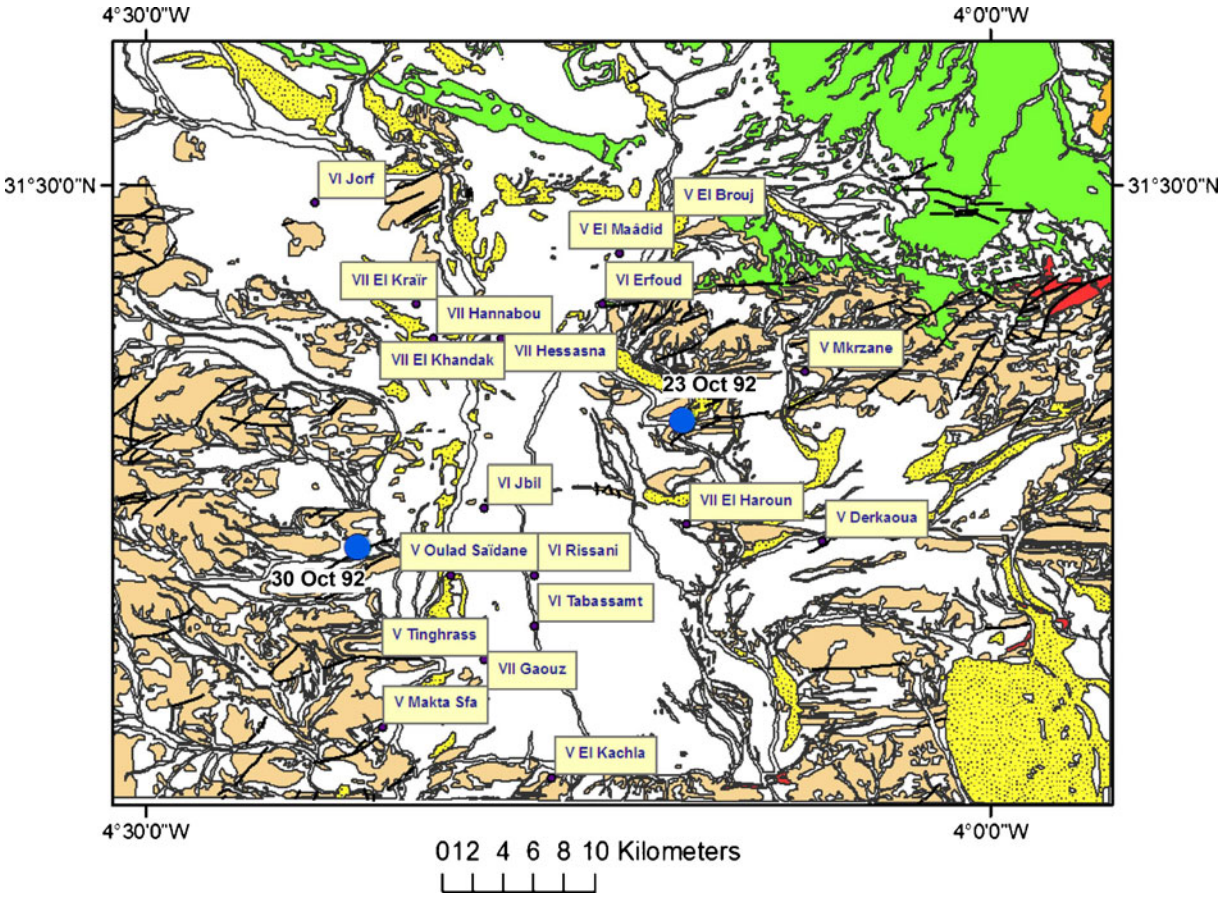

Fig. 5 Observed distribution of macroseismic intensity values for the shock of 30 October 1992, based on data collected by Cherkaoui (1993). *Blue circles* (1 and 2) show the epicentres of the 23 and 30 October shocks

oriented N–S and E–W (strike 9° and 277º) and very close to the vertical (dip 73° and 83º). The P and T axes are horizontal and oriented NW–SE and NE–SW. This solution is well constrained with estimation of axes errors less than 15º; the score is 1.0, but we have a lower number of observations (17 versus 30 for the 23 October shock). The dip of the E–W plane is tightly constrained by stations OUK and CHIE. Both planes are of opposite dip with respect to Harvard's solution.

Among the 305 aftershocks recorded by the temporary network installed by the Institut Scientifique it has been possible to estimate only the fault-plane solution for the earthquake that occurred on 6 November 1992 at 4 h 9 min, recorded at nine stations. The

Table 2 Parameters of the focal mechanism solutions determined by the present authors and Harvard

Event	Plane A (°) (Φ, δ, λ)	Plane B (°)	P axis (°) (Tr; pl)	T axis (°) (Tr; pl)	Method	Reference
23 October 1992	187; 69; 012	92; 78; 158	141; 07	048; 24	CMT	Harvard
	093; 82; 174	Not indicated	318; 01	048; 10	Waveform analysis	Jabour (1993)
	359±9; 71±9; –1±11	89±11; 89±10; –161±9	316±10; 14±10;	223±09; 13±09	FM	This paper
30 October 1992	090; 72; 176	181; 87; 018	314; 10	047; 15	CMT	Harvard
	9±11; 73±14; 7±11	277±12; 83±10; 163±14	324±12 07±12	232±11 16±12;	FM	This paper
6 November1992	207±116; 70±86; 005±20	115±27; 86±69; 159±115	163±113; 11±65	69±116; 18±68	FM	This paper

CMT Centroid Moment Tensor, *FM* P wave first motion, Φ strike, δ dip, λ slip, *Tr.* trend, *Pl.* plunge, *N* number of stations used

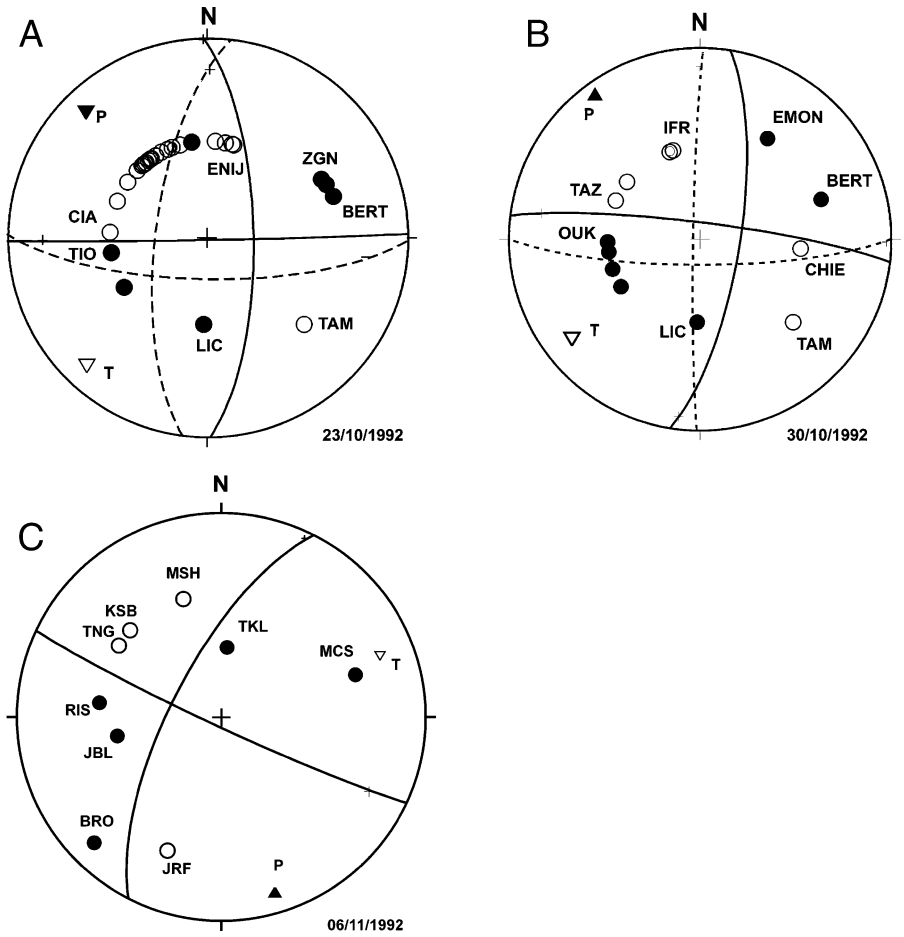

Fig. 6 Focal mechanisms (Schmidt net, lower hemisphere) of the 23 October 1992 (**a**), 30 October 1992 (**b**) and 6 November 1992, shocks. *Empty circles* dilatations; *full circles* compressions; *empty triangle* *T*-axis; *full triangle* *P*-axis

obtained solution (Table 2 and Fig. 6) corresponds also to strike-slip motion with a small reverse component, but the fault planes are oriented NNE–SSW and WNW–ESE. The P and T axes are horizontal and oriented NNW–SSE and ENE–WSW. In this case, estimation of errors for planes and stress axes is very high (Table 2) due to the low number of observations (9), despite the high score (1.00).

6 Scalar moment and source dimensions

The scalar seismic moment and source dimensions were estimated from spectral analysis using the model of Brune (1970). Data available correspond to four broadband stations located in Europe (FUR, AQUA and WET) and northern Africa (TAM) (Fig. 7 and Table 3) at epicentral distances between 12º and 23º. At lower distances, available data are analogical or digital short period.

The scalar seismic moment has been estimated using the amplitude spectra of P waves (Udias 1999). The radiation pattern for each station was computed from the fault plane solution estimated previously. From the corner frequency, we have estimated the dimensions using a circular model for the rupture. The average displacement and stress drop have been estimated from scalar moment and dimensions (Udias 1999).

The obtained scalar seismic moment (*Mo*) is similar for both events (Table 4), the 23 October event ($Mo=6.03\times10^{16}$ N m) being slightly larger than the 30 October shock ($Mo=5.03\times10^{16}$ N m). The corresponding values of *Mw* are 5.1 and 5.0, respectively.

For a circular fracture model, the dimensions of the faults ($2a$) are 7.7±1.4 and 7.4±1.2 km, respectively. From these values, and taking $\mu=3.2\times10^{4}$ MPa for both events, we obtain an average displacement of about 40 mm for the first event and 37 mm for the second one.

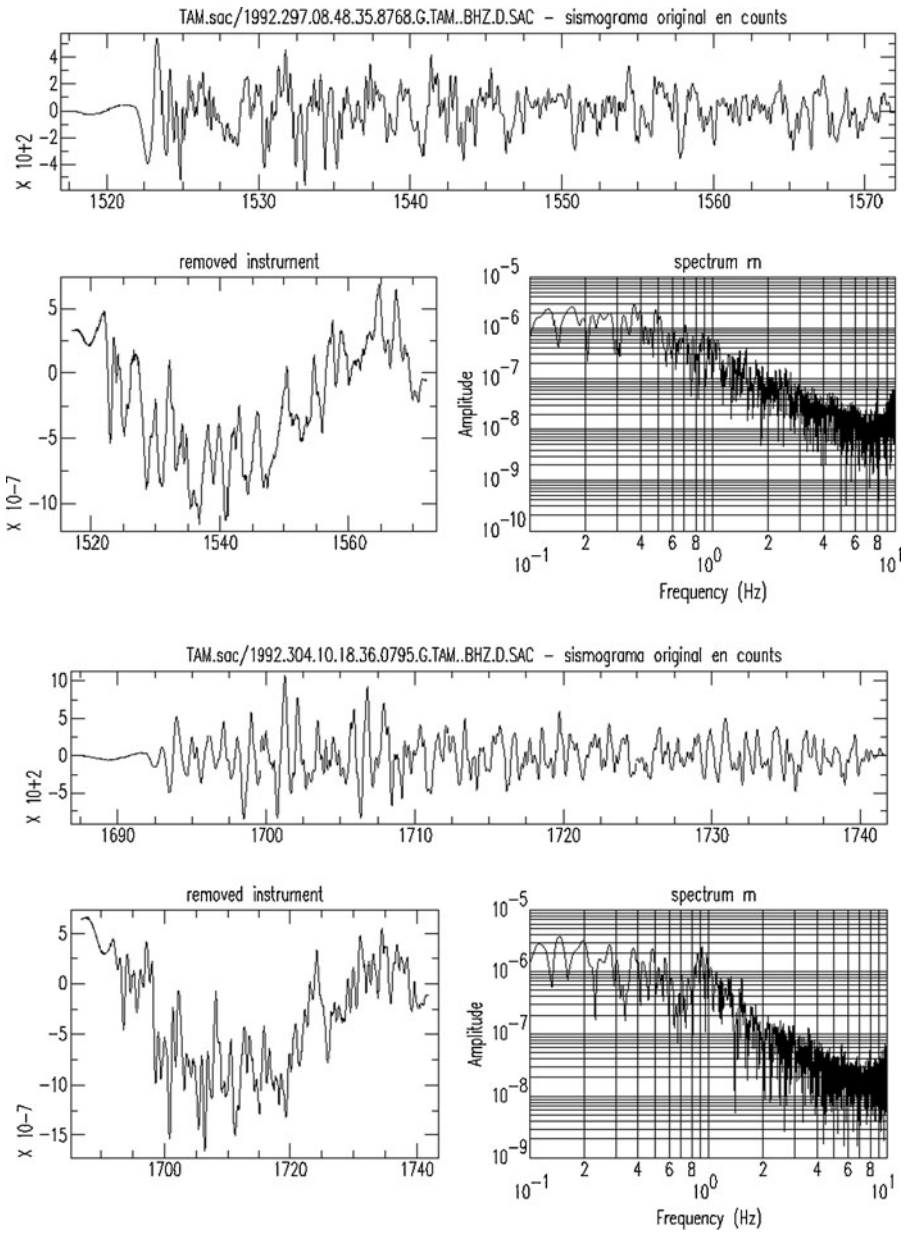

Fig. 7 Spectra of the 23 October (*upper panels*) and 30 October (*lower panels*) earthquake determined from the records of station TAM. *Top* original record; *bottom left* instrumental response removed; *bottom right* spectrum

The stress drop estimated using the expression:

$$\Delta\sigma = \frac{7M_o}{16a^3} \tag{2}$$

Where a is the source dimension, leads to values of 0.4 and 0.3 MPa, respectively, in agreement with standard values (Kanamori and Anderson 1975).

These results are somewhat different from those of Jabour (1993), who obtained for the 23 October event a scalar moment $Mo=0.008\times10^{25}$ dyn cm ($=8\times10^{16}$ N m), a dislocation of 5.6 cm and a stress drop of 7.8 bar (=0.78 MPa) using equation $\Delta\sigma=2.5\ Mo/S^{1.5}$ (S being the fault area).

Comparison between the records corresponding to the broadband stations for the 23 and 30 October earthquakes (Fig. 7) shows that both shocks have similar waveforms with the same amplitude and frequency. This confirms the similarity on the rupture process.

Table 3 Parameters of the stations used for the spectra, and results

Station	Δ (km)		Azimut		*Mo* Nm		*a* (km)	
	23/10/92	30/10/92	23/10/92	30/10/92	23/10/92	30/10/92	23/10/92	30/10/92
FUR	2439	2294	30.77	31.10	8.90×10^{16}	7×10^{16}	4.47	4.47
AQU	1980	1980	47.31	47.59	11.46×10^{16}	8.78×10^{16}	2.79	2.79
WET	2439	2454	31.17	31.47	1.66×10^{16}	2.97×10^{16}	3.72	3.72
TAM	1350	1357	132.33	131.55	2.10×10^{16}	1.27×10^{16}	3.72	2.79

Δ epicentral distance, *Mo* seismic moment, *a* rupture length

7 Discussion

7.1 Area of largest damage vs instrumental epicentres

The largest damage (*I*=VII and VI MSK64) was observed over an area of 2,000 km² (*ksour* of Hessasna, El Khandek, Hannabou, El Kraïr and El Bouiya (Fig. 5)) located close to the epicentres of the 23 and 30 October shocks. Comparison of the local intensities to the geological and topographic maps shows that the area of largest damage clearly does not match the instrumental epicentres (Fig. 5); therefore, we infer that the damage may have also been a consequence of a site effect, involving amplification of the seismic waves by the Quaternary sediments of the valley. Liquefaction of sediments beneath the villages was not observed but is highly probable to have occurred, given that the water table is at shallow depth, in the range 4–20 m only (Margat et al. 1962; Ruhard 1977) and that some observations reported rising of the water level of wells in several localities along the Ziz river (Cherkaoui 1993).

7.2 Relationship between both earthquakes

7.2.1 Structural and seismic considerations

Because of the lack of structural field studies after the occurrence of the earthquakes and the few aftershock data available, a precise seismotectonic model cannot be proposed for the seismic crisis of 1992. However, we attempt a tentative model based on the following considerations:

1. The shallow character of foci (2 km depth) and the strike-slip motion with near-vertical faults oriented N–S and E–W exclude the intra-crustal gently dipping detachment faults (Wigger et al. 1992) as possible sources of the main shocks of Rissani.
2. In addition, as no N–S faults were observed on the seismic profiles, the major faults in the area have a predominantly E–W strike. The two major faults with this strike are the Erfoud Fault, and the fault running across the line Rissani-El Haroune line, at the centre of the section in Fig. 2b. As the Erfoud fault seems to have remained inactive during the seismic crisis, the Rissani-El Haroune fault appears to be the one that generated the earthquakes.
3. Despite large horizontal uncertainties, the two main epicentres are aligned along the Rissani-El Haroun trend.
4. The first shock was not followed by any aftershock sequence, so we suppose that the displacement created by the first shock was not accommodated immediately, but after one week by the second shock.
5. Almost all aftershocks are located west of Rissani, an area corresponding to the probable westward termination of the Rissani-El Haroune fault line. Therefore, they should be interpreted as a compressional tip line of the E–W fault, as attested by the focal mechanism of the largest aftershock.

Table 4 Source parameters calculated from the spectra

Event	*Mo* (Nm)	*Mw*	*2a* (km)	N	Δ*u* (cm)	Δσ (MPa)
23 October 1992	6.03×10^{16}	5.1	7.73+1.38	4	4	0.4
30 October 1992	5.07×10^{16}	5.0	7.36+1.2	4	3.7	0.3

Mo seismic moment, *Mw* moment magnitude, *2a* rupture length, Δ*u* displacement along the fault, *Δσ*, stress drop

7.2.2 Coulomb stress failure test

It is well known that earthquakes occur when fault stresses increase to levels that exceed a critical threshold for fault rupture (e.g. Scholz 1990). Several studies reveal that any additional stress to a fault system may initiate the rupture process that produces an earthquake. Harris et al. (1995) inferred that >0.1 bar of transferred stress was capable of triggering earthquakes; Stein et al. (1994) affirm that moderate strike-slip earthquakes can occur in regions where the stress change on optimally oriented vertical faults is increased by >0.3 bar; Métivier et al. (2009) find that the additional stresses, with magnitudes less than 0.04 bar, produced by Earth's tides, might also trigger earthquakes.

In order to test the previous assumptions, Coulomb Stress Change (CSC) has been estimated through Coulomb programme (Toda et al. 2005; Lin and Stein 2004) considering the parameters listed in Table 4 and rigidity $\mu=3.2\times10^4$ MPa, Poisson's ratio=0.25 and Young modulus=8×10^5 bar, values habitually used in this type of calculus (Freed and Lin 2001). To estimate the CSF, we needed considering rectangular sources with the same area than those calculated from Brune model (S1=48 km^2=8×6 km; S2=36 km^2=6×6 km).

In a first attempt, the results performed combining the four planes obtained from focal mechanisms (Table 2) show that in the four cases, the stress field changes produced by the first event have low values (~0.02 bar) at the proximity of the second event source. Figure 8a shows the case in which the E–W planes are considered. This may be due to the low moment magnitude (*Mw*) of earthquakes (~5) and the too large distance between the determined epicentres (17.7 km).

In a second attempt, CSC was calculated taking into account the estimated horizontal errors in the location (Table 1). The new coordinates used are 31.341° N; 4.217° W (23 October) and 31.317° N; 4.301° W (30 October), and the distance between both epicentres decreases to 9 km. Three cases were considered using the E–W planes (Fig. 8b–d):

1. In case 1 (Fig. 8b), stress change produced from the source 1 on a horizontal plane at 2 km depth, considering receiver sources with geometry as in source 2, shows the increase of stress in hypocenter region of the 30 Oct. earthquake (~0.3 bar) that favours the rupture.
2. In case 2 (Fig. 8c), the maximum stress change produced from source 1 to a range of horizontal planes between 0 and 20 km depth, and a fault geometry as source 2 (receiver source), shows an increase of Coulomb stress of ~0.3 bar to the 30 October considered epicentre. The equality between the obtained values in cases 1 and 2 confirms to be the 2 km the more probable depth to the event of 30 October.
3. Case 3 (Fig. 8d) shows the maximum stress change produced from the two sources together to a range of horizontal planes between 0 and 20 km depth to a characteristic receiver source and the aftershocks recorded.

The tested cases show that the Coulomb stress field change produced by the 23 October event is considerable and positive (~0.3 bar) in the proximity of the 30 October event. So, by this calculus, we can admit that the 23 October event may have induced the 30 October earthquake. However, the aftershocks do not match correctly the areas of positive increase of stress, which may be related to location of the main shocks.

7.3 Thermal and tectonic components of the Anti-Atlas relief

As presented in sections 1–3, the Anti-Atlas is generally considered as a foreland chain, tightly related to the inversion of the High Atlas Triassic–Jurassic rift during the Tertiary and the Quaternary. Geophysical studies based on seismic tomography (Seber et al. 1996) and modelling of geothermal, topographic and gravity data (Teixell et al. 2005; Missenard et al. 2006) have suggested that a large asthenospheric dome extends across the Anti-Atlas from the Canary Islands to Northern Morocco. As a consequence, the uplift of the Anti-Atlas is considered to be mainly related to the thermal anomaly (Frizon de Lamotte et al. 2009), or involving a small tectonic component (one third of the total relief), as can be inferred from the differences in topography obtained with or without a thermal component (Missenard et al. 2006). The concept of a neotectonic stability is clearly questioned by Zouhri et al. (2008), based on the observation of seismites in the Miocene deposits at Tourt. In addition, the occurrence of large wavelength deformation of the sub-Saharan lithosphere

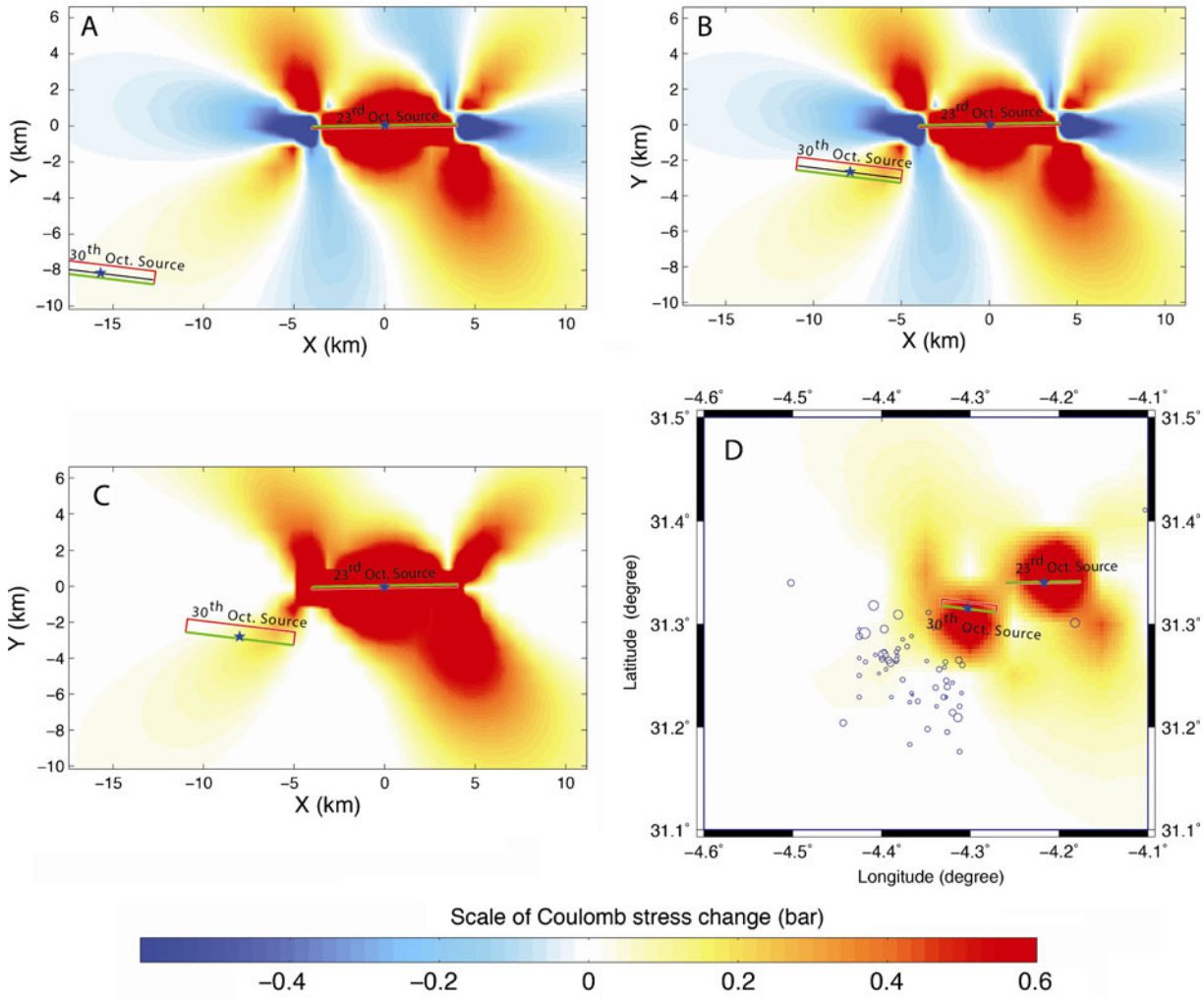

Fig. 8 Coulomb stress tests for the Rissani earthquakes. **a** Case in which the E–W planes are considered using the original coordinates: 31.361° N; 4.182° W (23 October) and 31.286° N; 4.347° W (30 October). **b**–**d** CSF calculated taking into account the estimated horizontal errors in the location (Table 1) and new coordinates 31.341° N; 4.217° W (source 1: 23 October) and 31.317° N; 4.301° W (source 2: 30 October) which reduce the distance between both epicentres to 9 km; **b** stress change produced from the source 1 on a horizontal plane at 2 km depth, and a fault geometry as in source 2 (receiver source); **c** maximum stress change produced from source 1 to a range of horizontal planes between 0 and 20 km depth, and a fault geometry as source 2 (receiver source); **d** maximum stress change produced from the two sources together to a range of horizontal planes between 0 and 20 km depth and to a characteristic receiver source and location of aftershocks

during the Late Cretaceous-Neogene is considered as a far field effect of the Atlas orogeny, namely a compressive deformation of the sub-Saharan lithosphere (Frizon de Lamotte et al. 2009).

The occurrence of the Rissani earthquakes implies that a seismo-tectonic component should be taken into account in the build-up of the chain. The main problem is that there is little knowledge on the history of earthquakes in the area, because of the lack of historical studies and probably because the low density of population in these pre-Saharan areas, due to a nomad way of life until recent times. Also, the recurrence period of such events is certainly larger than the instrumental period (110 years).

It can be argued that the strike-slip motion determined cannot produce any relief, and thus do not contribute to uplift. However, (1) in the case of the Tafilalt crisis, the inferred fault plane is oblique to the NW–SE trending regional maximum compressive stress in Morocco (see references in section 1); (2) the

focal mechanisms are similar to those determined in the High Atlas (Medina and Cherkaoui 1992; Medina 2008), which has undergone considerable uplift; (3) it is certain that there has been recent reverse faulting which produced (small) relief as recorded in the Ouarzazate basin (Sébrier et al. 2006); (4) it is difficult to observe recent faulting and relief increase in the axial zone of the Anti-Atlas chain because of the absence of depositional features; therefore, only a detailed morphologic study comparable to that of Joly (1962) could lead to a better knowledge of the neotectonics of the area.

8 Conclusions

The review of the data available on the Tafilalt seismic crisis of October–November 1992 allowed us to precise the macroseismic, instrumental and hence the source parameters of the major earthquakes. The main results of the present study are:

1. Relocation with the help of a close portable network allowed us to propose new epicentral coordinates, which are 31.361° N; 4.182° W (23 October) and 31.286° N; 4.347° W (30 October). Both events have focal depths of 2 km.
2. The shock of 30 October was followed by a series of 305 aftershocks mostly located west of Rissani, 61 of them having depths of 5 to 19 km and magnitudes 0.7 to 3.
3. The largest damage, attaining VII on MSK64 scale, was observed in an area located between the two epicentres within the valley and may have been increased by site effects due to the proximity of the water table.
4. Focal mechanisms of the main events correspond to strike-slip faulting with the fault planes oriented N–S (left lateral) and E–W (right lateral). The only mechanism available for the aftershocks also corresponds to strike-slip faulting.
5. Spectral analysis shows that scalar seismic moment (*Mo*) of the first event is slightly larger than the second. The corresponding values of *Mw* are 5.1 and 5.0, respectively.
6. The dimensions of the faults for a circular fault model are 7.7±1.4 and 7.4±1.2 km, respectively. From these values, we obtained an average displacement of 4 cm for the first event and 3.7 cm for the second. The stress drop is 0.4 and 0.3 MPa, respectively, in agreement with standard values.
7. The Coulomb Stress test performed for both earthquakes suggests a relationship between both events only when the used location is at the limit of the horizontal uncertainty.
8. Finally, this crisis suggests that the Anti-Atlas is undergoing tectonic deformation, and not only thermal uplift, as suggested by recent publications.

Acknowledgements This study has been partially supported by the Universidad Complutense de Madrid, project AE1/09-16586 to I. Bensaid and E. Buforn. We are particularly indebted to Pr. Denis Hatzfeld (IRIGM, Observatory of Grenoble) for providing the seismograms of the microseismic campaign carried out in the Khénifra province in collaboration with the Scientific Institute (T.-E. Cherkaoui), to two anonymous reviewers for their valuable comments which helped improving the manuscript, and to Prof. Lahsen Baidder (University Hassan II–Casablanca) for sending us useful documentation. We acknowledge the help of several colleagues in Tunisia, Ivory Coast and France, who gently provided copies of seismograms. We thank M'hamed Bikraoui, Mohamed Laami (technicians) and Abderrahim El Alaoui and Lakbir El Bekraoui for their help in the fieldwork during the survey of 1992. The local authorities and the Royal Gendarmery provided valuable help in the field. Finally, Hind El Hachimi and Nadia Mhammdi kindly helped us in preparing the first draft of the structural map of Tafilalt.

References

Baidder L (2007) Structuration de la bordure septentrionale du Craton Ouest-Africain du Cambrien à l'Actuel: cas de l'Anti-Atlas oriental du Maroc. Thèse d'Etat Univ Hassan II-Aïn Chock, Fac Sci Casablanca

Baidder L, Raddi Y, Tahiri M, Michard A (2008) Devonian extension of the Pan-African crust north of the West African craton, and its bearing on the Variscan foreland deformation: evidence from eastern Anti-Atlas (Morocco). In: Ennih N, Liégeois JP (eds) The boundaries of the West African Craton. Geol Soc, London, pp 453–465, sp pub 297

Ben Sari D (1978) Connaissance géophysique du Maroc. Thèse d'Etat, Grenoble

Bensaid I, Medina F, Cherkaoui T-E, Buforn E, Hahou Y (2009) New P-wave first motion solutions for the focal mechanisms of the Rissani (Morocco) earthquakes of October 23^{d} and 30th, 1992. Bull Inst Sci, Rabat, sect Sci Terre 31:55–59

Bezzeghoud M, Buforn E (1999) Source parameters of the 1992 Melilla (Spain, Mw=4.8), 1994 Alhoceima (Morocco, Mw=5.8) and 1994 Mascara (Algeria, Mw=5.7) earthquakes and seismotectonic implications. Bull Seismol Soc Am 89:359–372

Brillinger DR, Udias A, Bolt BA (1980) A probability model for regional focal mechanism solutions. Bull Seism Soc Am 70:149–170

Brune JN (1970) Tectonic stress and the spectra of seismic shear waves from earthquakes. J Geophys Res 75 (26):4997–5009

Buforn E, Udias A (2010) Azores-Tunisia, a tectonically complex boundary. In: Dmowska R (ed) Adv Geophys, 52, pp 139–182

Buforn E, Sanz de Galdeano C, Udias A (1995) Seismotectonics of the Ibero-Maghrebian region. Tectonophysics 152:89–118

Buforn E, Bezzeghoud M, Udias A, Pro C (2004) Seismic sources on the Iberia-African plate boundary and their tectonic implications. Pure Appl Geophys 161(3):623–646

Chalouan A, Galindo-Zaldívar J, Akil M, Marín C, Chabli A, Ruano P, Bargach K, Sanz de Galdeano C, Benmakhlouf M, Ahmamou M, Gourari L (2006) Tectonic wedge escape in the southwestern front of the Rif Cordillera (Morocco). In: Moratti G, Chalouan A (ed) Tectonics of the Western Mediterranean and North Africa. Geological Society of London, special publication 262, pp 101–118

Cherkaoui T-E (1988) Fichier des séismes du Maroc et des régions voisines 1901–1984. Trav Inst Sci, sér Géol Géogr phys 17:1–168

Cherkaoui T-E (1991) Contribution à l'étude de l'aléa sismique au Maroc. Thesis. University Joseph Fourier, Grenoble (France)

Cherkaoui T-E (1993) Etude sismologique du séisme du 30 octobre 1992 à Rissani. Rapport inédit, Dpt Phys Globe, Inst Sci, Univ. Mohammed V, Rabat

Choubert G, Fallot P, Marçais G, Suter G, Tilloy R (1946–1955) Carte géologique du Maroc au 1/500.000. Service géologique du Maroc

de Vicente G, Cloetingh S, Muñoz-Martın A, Olaiz, A, Stich D, Vegas R, Galindo-Zaldıvar J, Fernandez-Lozano J (2008) Inversion of moment tensor focal mechanisms for active stresses around the microcontinent Iberia: Tectonic implications. Tectonics, 27, TC1009, doi:10.1029/2006TC002093

DeMets C, Gordon RG, Argus DF (2010) Geologically current plate motions. Geophys J Intern 181:1–80

Destombes J, Hollard H (1986) Carte géologique du Maroc au 1/200000, feuille Tafilalt-Taouz. Notes Mém Serv Géol Maroc, 244

El Alami SO, Tadili B, Aït Brahim L, Mouayn I (2004) Seismicity of Morocco for the period 1987–1994. Pure appl Geophys 161:969–982

Elmrabet T (2005) Les tremblements de terre majeurs dans la région du Maghreb, et leurs conséquences sur l'homme et l'environnement. Ed. CNRST-LAG, Rabat [in arabic]

Fadil A, Vernant P, McClusky S, Reilinger R, Gomez F, Ben Sari D, Mourabit T, Feigl K, Barazangi M (2006) Active tectonics of the western Mediterranean: geodetic evidence for rollback of a delaminated subcontinental lithospheric slab beneath the Rif Mountains, Morocco. Geology 34 (7):529–532

Freed AM, Lin J (2001) Delayed triggering of the 1999 Hector Mine earthquake by viscoelastic stress transfer. Nature 411:180–183

Frizon de Lamotte D, Leturmy P, Missenard Y, Khomsi S, Ruiz G, Saddiqi O, Guillocheau F, Michard A (2009) Mesozoic and Cenozoic vertical movements in the Atlas system (Algeria, Morocco, Tunisia): An overview. Tectonophysics 475:9–28

Frogneux M (1980). La sismicité marocaine de 1972 à 1978. Etude des paramètres à la source des séismes proches. Thèse de Troisième Cycle, Univ Grenoble

Gasquet D, Ennih N, Liégeois J-P., Soulaimani A, Michard A (2008) The Pan-African belt. In: Michard A, Saddiqi O, Chalouan A, Frizon de Lamotte D (eds) Continental evolution: the Geology of Morocco. Structure, stratigraphy and tectonics of the Africa-Atlantic-Mediterranean triple junction. Springer, Lecture Notes in Earth Sciences, 116, pp 33–64

Giese P, Jacoshagen V (1992) Inversion tectonics of intracontinental ranges: High and Middle Atlas, Morocco. Geol Rundsch 81:249–259

Hahou Y (2005) Sismicité du Maroc; apport de l'étude des séismes d'Al Hoceima et de Rissani et évaluation du risque sismique. Thèse de Doctorat, Univ Mohammed V-Agdal, Fac Sci Rabat

Hahou Y, Jabour N, Oukemeni D, El Wartiti M (2003) The October 23; 30, 1992 Rissani earthquakes in Morocco: Seismological, macroseismic data. Bull Int Inst Seismol Earthq Eng, Special Edition, pp 85–94

Harris RA, Simpson RW, Reseanberg PA (1995) Influence of static stress changes on earthquake locations in Southern California. Nature 375:221–224

Hatzfeld D (1978) Etude sismotectonique de la zone de collision Ibéro-Maghrébine. Thèse d'Etat. University Joseph Fourier, Grenoble

Hatzfeld D, Frogneux M (1981) Intermediate depth seismicity in the western Mediterranean unrelated to subduction of oceanic lithosphere. Nature 292:443–445

Henares J, López Casado C, Sanz de Galdeano C, Delgado J, Peláez JA (2003) Stress fields in the Iberian-Maghrebi region. J Seismol 7:65–78

International Seismological Centre (1992) Bulletin, October 1992, Kew (U.K.), pp 202–203, 353–355

Jabour N (1993) Source process of earthquakes in the Atlantic Ocean and Morocco. Intern Inst Seismol Earthq Engineering, individual studies, course 1992–1993, vol 29, 13 p

Joly F (1962) Etudes sur le Relief du Sud-Est marocain. Trav Inst Sci, sér Géol Géogr phys 10:1–578

Kanamori H, Anderson DL (1975) Theoretical basis of some empirical relations in seismology. Bull Seismol Soc Am 65(5):1073–1095

Lee WHK, Valdés CM (1985) HYPO71PC: a personal computer version of the HYPO71 earthquake location program. US Geol Surv Open-File Report 85–749

Lin J, Stein RS (2004) Stress triggering in thrust and subduction earthquakes, and stress interaction between the southern San Andreas and nearby thrust and strike-slip faults. J Geophys Res 109:B02303. doi:10.1029/2003JB002607

Malusà MG, Polino R, Cerrina Feroni A, Ellero A, Ottria G, Baidder L, Musumeci G (2007) Post-Variscan tectonics in eastern Anti-Atlas (Morocco). Terra Nova 19(6):481–489

Margat J (1960) Carte hydrogéologique de la plaine du Tafilalt. I- Géologie et piézométrie. Publ Serv Géol Maroc, n 150

Margat J, Destombes J, Hollard H (1962) Mémoire explicatif de la Carte hydrogéologique au 1/50000 de la plaine de Tafilalt. Notes Mém Serv géol Maroc, n 150 bis

McClusky S, Reilinger R, Mahmoud S, Ben Sari D, Tealeb A (2003) GPS constraints on Africa (Nubia) and Arabia plate motions. Geophys J Int 155:126–138

Medina F (1995) Present-day state of stress in northern Morocco from focal mechanism analysis. J Struct Geol 17:1035–1046

Medina F (2008) Catalogue of focal mechanisms of the Moroccan earthquakes for the period 1959–2007. Doc Inst Sci 22:1–56

Medina F, Cherkaoui TE (1992) Mécanismes au foyer des séismes du Maroc et des régions voisines (1959–1986). Conséquences tectoniques Eclogae Geol Helv 85(2):433–457

Medina F, El Alami SO (2006) Focal mechanisms and state of stress in the Al Hoceima area (Central Rif, Morocco). Bull Inst Sci, Rabat, sect Sci Terre 28:19–30

Métivier L, Viron O, Conrad CP, Renault S, Diament M, Patau G (2009) Evidence of earthquake triggering by the solid earth tides. Earth Planet Sci Lett 278:370–375

Michard A, Hoepffner C, Soulaimani A, Baidder L (2008) The Variscan belt. In: Michard A, Saddiqi O, Chalouan A, Frizon de Lamotte D (eds) Continental evolution: the Geology of Morocco. Structure, stratigraphy and tectonics of the Africa-Atlantic-Mediterranean triple junction. Springer, ser. Lecture Notes in Earth Sciences 116:65–132

Missenard T, Zeyen H, Frizon de Lamotte D, Leturmy P, Petit C, Sébrier M, Saddiqi O (2006) Crustal versus asthenospheric origin of relief of the Atlas Mountains of Morocco. J Geophys Res 111:B03401. doi:10.1029/2005JB003708

Pedrera A, Ruiz-Constán A, Galindo-Zaldívar J, Chalouan A, Sanz de Galdeano C, Marín-Lechado C, Ruano P, Benmakhlouf M, Akil M, López-Garrido AC, Chabli A, Ahmamou M, González-Castillo L (2011) Is there an active subduction beneath the Gibraltar orogenic arc? Constraints from Pliocene to present-day stress field. J Geodyn (in press)

Plaziat J-C, Aberkan M, Ahmamou M, Choukri R (2008) The Quaternary deposits of Morocco. In: Michard A, Saddiqi O, Chalouan A, Frizon de Lamotte D (eds): Continental evolution: the Geology of Morocco. Structure, stratigraphy and tectonics of the Africa-Atlantic-Mediterranean triple junction. Springer, ser. Lecture Notes in Earth Sciences 116:359–376

Robert-Charrue C, Burkhard M (2008) Inversion tectonics interference pattern and extensional fault-related folding in the Eastern Anti-Atlas, Morocco. Swiss J Geosci 101:397–408

Rousseau L, Beauchamp J, Bahain J-J, Boudad L, Deschamps P, Falguères C, Ghaleb B, Lartigot A-S, Pozzi J-P (2006) Premiers résultats d'une étude pluridisciplinaire menée sur des travertins quaternaires du Maroc. Quaternaire 17 (4):343–350

Roux G (1934) Notes sur les tremblements de terre ressentis au Maroc avant 1933. Mém Soc Sci Nat Maroc, XXXIX:42–71

Ruhard J-P (1977) Le bassin quaternaire du Tafilalt. In: Ressources en eau du Maroc, tome 3: Domaines atlasique et sud-atlasique. Notes Mém Serv géol Maroc 231:352–415

Scholz CH (1990) The Mechanics of Earthquakes and Faulting. Cambridge Univ Press, New York

Schwarz G, Wigger PJ (1988) Geophysical studies of the Earth's crust and upper mantle in the Atlas system of Morocco. In: Jacobshagen VH (Ed) The Atlas system of Morocco; studies on its geodynamic evolution. Springer-Verlag, Lecture Notes in. Geosciences 15:339–357

Schwarz G, Mehl HG, Ramdani F, Rath V (1992) Electrical resistivity structure of the eastern Moroccan Atlas system and its tectonic implications. Geol Rundsch 81(1):221–235

Seber D, Barazangi M, Tadili BA, Ramdani M, Ibenbrahim A, Ben Sari D (1996) Three dimensional upper mantle structure beneath the intraplate Atlas and interplate Rif mountains of Morocco. J Geophys Res 101:3125–3138

Sébrier M, Siame L, Zouine EM, Winter T, Missenard Y, Leturmy P (2006) Active tectonics in the Moroccan High Atlas. CR Geosciences 338(1–2):65–79

Stein RS, King GCP, Lin J (1994) Stress triggering of the 1994 M=6.7 Northridge, California, earthquake by its predecessors. Science 265:1432–1435

Stich D, Serpelloni E, Mancilla F, Morales J (2006) Kinematics of the Iberia—Maghreb plate contact from seismic moment tensors and GPS observations. Tectonophysics 426:295–317

Tahayt A, Feigl KL, Mourabit T, Rigo A, Reilinger R, McClusky S, Fadil A, Berthier E, Dorbath L, Serroukh M, Gomez F, Ben Sari D (2009) The Al Hoceima (Morocco) earthquake of 24 February 2004, analysis and interpretation of data from ENVISAT ASAR and SPOT5 validated by ground-based observations. Rem Sens Environ 113:306–316

Teixell A, Ayarza P, Zeyen H, Fernandez M, Arboleya ML (2005) Effects of mantle upwelling in a compressional setting: the Atlas Mountains of Morocco. Terra Nova 17:456–461

Toda S, Stein RS, Richards-Dinger K, Bozkurt S (2005) Forecasting the evolution of seismicity in southern California: Animations built on earthquake stress transfer. J Geophys Res, B05S16, doi:10.1029/2004JB003415

Toto EA, Kaabouben F, Zouhri L, Belarbi M, Benammi M, Hafid M, Boutib L (2007) Geological evolution and structural style of the Palaeozoic Tafilalt sub-basin, eastern Anti-Atlas (Morocco, North Africa). Geol J. doi:10.1002/gj.1098

Udias A (1999) Principles of Seismology. Cambridge University Press

Vernant P, Fadil A, Mourabit T, Ouazar D, Koulali A, Davila JM, Garate J, McClusky S, Reilinger R (2010) Geodetic constraints on active tectonics of the Western Mediterranean: Implications for the kinematics and dynamics of the Nubia-Eurasia plate boundary zone. J Geodyn 49(3–4):123–129

Wigger P, Asch G, Giese P, Heinsohn W-D, El Alami SO, Ramdani F (1992) Crustal structure along a traverse across the Middle and High Atlas mountains derived from seismic refraction studies. Geol Rundsch 81(1):237–248

Zouhri S, Kchikach A, Saddiqi O, El Haïmer FZ, Baidder L, Michard A (2008) The Cretaceous-Tertiary plateaus. In: Michard A, Saddiqi O, Chalouan A, Frizon de Lamotte D (eds) Continental evolution: the Geology of Morocco. Structure, stratigraphy and tectonics of the Africa-Atlantic-Mediterranean triple junction. Springer, ser. Lecture Notes in Earth Sciences, 116, pp 331–358